1114 *Chem. Mater.* **2010,** *22,* 1114–1118
DOI:10.1021/cm902272q

CHEMISTRY OF MATERIALS
Article

TiO_2 Branched Nanostructure Electrodes Synthesized by Seeding Method for Dye-Sensitized Solar Cells†

Jae-Kyung Oh, Jin-Kyu Lee, Hyun-Su Kim, Sang-Beom Han, and Kyung-Won Park*

Department of Chemical and Environmental Engineering, Soongsil University, Seoul 156-743, Korea

Received July 24, 2009. Revised Manuscript Received October 21, 2009

We report TiO_2 branched nanostructure photoelectrodes for dye-sensitized solar cells (DSSCs). The TiO_2 branch-type nanoparticle is synthesized by means of a seeding method with TiO_2 nanowire as a seed. During the seeding process, the TiO_2 nanostructure is evolved from a nanowire (NW) to nanobranch (NB) shape. It is also found that rutile TiO_2-NB shows such a three-dimensional structure with branches grown along backbones of rutile TiO_2-NW as confirmed by high-resolution transmission electron microscopy (HR-TEM) and X-ray diffraction (XRD) analysis. In photocurrent−voltage measurements, short-circuit current density, and cell efficiency of TiO_2-NW and TiO_2-NB increase from 6.25 to 12.18 mA/cm^2 and increase from 2.6 to 4.3%, respectively, due to both increased specific surface area and roughness factor.

Introduction

Titanium oxide (TiO_2) has been an attractive material for a variety of applications such as dye-sensitized solar cells (DSSCs),[1,2] photocatalysts,[3,4] sensors,[5] splitting of water,[6] lithium ion batteries,[7] and direct methanol fuel cells (DMFCs).[8,9] TiO_2 exists in crystal structures such as anatase, rutile and brookite. However, in particular, the rutile phase has some advantages over the anatase phase such as higher chemical stability, higher refractive index, and cheaper cost of production.[10,11]

Dye-sensitized solar cells have been attractive, because of the low cost and relatively high conversion efficiency, in the followng fields dye as the injection of the photo-excited electron, liquid electrolytes such as I^-/I_3^- redox couples, counter electrodes for iodine reduction and nanocrystalline TiO_2 photoelectrode. Especially, the photoelectrode consists of TiO_2 nanoparticles on a transparent conducting glass to achieve a high specific surface area for adsorption of dye molecules. However, the low diffusion coefficients of TiO_2 particles can be understood by the hypothesis of electron traps in the porous electrode. The defects in the porous TiO_2 electrode could act as electron trap sites resulting from interconnection between nanoparticles. Thus, it is expected that one-dimensional structures such as nanowires, nanorods, or nanotubes in comparison with spherical nanoparticles can result in an improved electron transport during the solar energy conversion process.[12−15]

Among the one-dimensional nanostructures, the nanowire electrode shows particular properties such as rapid electron collection of carriers and charge transport assisted by its one-dimensional structure.[16−18] However, the one-dimensional nanostructure electrode has a tendency to lie in the plane of the film, which is not favorable in an optimum arrangement for an electron extraction. Accordingly, many research groups have reported branched nanostructures prepared by means of the vapor−liquid−solid (VLS) growth method and wet chemical process.[19−24]

† Accepted as part of the 2010 "Materials Chemistry of Energy Conversion Special Issue".

*Corresponding author. Tel.: 82-2-820-0613. Fax: 82-2-812-5378. E-mail address: kwpark@ssu.ac.kr.

(1) O'Reagen, B.; Grätzel, M. *Nature* **1991**, *353*, 737–740.
(2) Grätzel, M. *Inorg. Chem.* **2005**, *44*(20), 6841–6851.
(3) Zhang, Z.; Wang, C.-C.; Zakaria, R.; Ying, J. Y. *J. Phys. Chem. B* **1998**, *102*(52), 10871–10878.
(4) Kominami, H.; Murakami, S.-y.; Kato, J.-i.; Kera, Y.; Ohtani, B. *J. Phys. Chem. B* **2002**, *106*(40), 10501–10507.
(5) Zhu, Y.; Shi, J.; Zhang, Z.; Zhang, C.; Zhang, X. *Anal. Chem.* **2002**, *74*(1), 120–124.
(6) Fujishima, A.; Honda, K. *Nature* **1972**, *238*, 37–38.
(7) Tarascon, J.-M.; Armand, M. *Nature* **2001**, *414*, 359–367.
(8) Park, K.-W.; Han, S.-B.; Lee, J.-M. *Electrochem. Commun.* **2007**, *9*(7), 1578–1581.
(9) Park, K.-W.; Seol, K.-S. *Electrochem. Commun.* **2007**, *9*(9), 2256–2260.
(10) Hosono, E.; Fujihara, S.; Kakiuchi, K.; Imai, H. *J. Am. Chem. Soc.* **2004**, *126*(25), 7790–7791.
(11) Hoffmann, M. R.; Martin, S. T.; Choi, W.; Bahnemann, D. W. *Chem. Rev.* **1995**, *95*(1), 69–96.
(12) Koo, B.; Park, J.; Kim, Y.; Choi, S.-H.; Sung, Y.-E.; Hyeon, T. *J. Phys. Chem. B* **2006**, *110*(48), 24318–24323.
(13) Adachi, M.; Murata, Y.; Takao, J.; Jiu, J.; Sakamoto, M.; Wang, F. *J. Am. Chem. Soc.* **2004**, *126*(45), 14943–14949.
(14) Kang, S. H.; Kim, J.-Y.; Sung, Y.-E. *Electrochim. Acta* **2007**, *52*(16), 5242–5250.
(15) Liu, B.; Aydil, E. S. *J. Am. Chem. Soc.* **2009**, *131*(11), 3985–3990.
(16) Kang, S. H.; Choi, S.-H.; Kang, M.-S.; Kim, J.-Y.; Kim, H.-S.; Hyeon, T.; Sung, Y.-E. *Adv. Mater.* **2008**, *20*(1), 54–58.
(17) Law, M.; Greene, L. E.; Johnson, J. C.; Saykally, R.; Yang, P. *Nat. Mater.* **2005**, *4*, 455–459.
(18) Li, W.-J.; Shi, E.-W.; Yin, Z.-W. *J. Cryst. Growth* **2000**, *208*(1−4), 546–554.
(19) Sun, B.; Marx, E.; Greenham, N. C. *Nano Lett.* **2003**, *3*(7), 961–963.
(20) Gur, I.; Fromer, N. A.; Chen, C.-P.; Kanaras, A. G.; Alivisatos, A. P. *Nano Lett.* **2007**, *7*(2), 409–414.
(21) Suh, D.-I.; Lee, S.-Y.; Kim, T.-H.; Chun, J.-M.; Suh, E.-K.; Yang, O.-B.; Lee, S.-K. *Chem. Phys. Lett.* **2007**, *442*(4−6), 348–353.
(22) Jung, Y.; Ko, D.-K.; Agarwal, R. *Nano Lett.* **2007**, *7*(2), 264–268.
(23) Sounart, T. L.; Liu, J.; Voigt, J. A.; Huo, M.; Spoerke, E. D.; McKenzie, B. *J. Am. Chem. Soc.* **2007**, *129*(51), 15786–15793.
(24) Dong, A.; Tang, R.; Buhro, W. E. *J. Am. Chem. Soc.* **2007**, *129*(40), 12254–12262.

Published on Web 11/02/2009

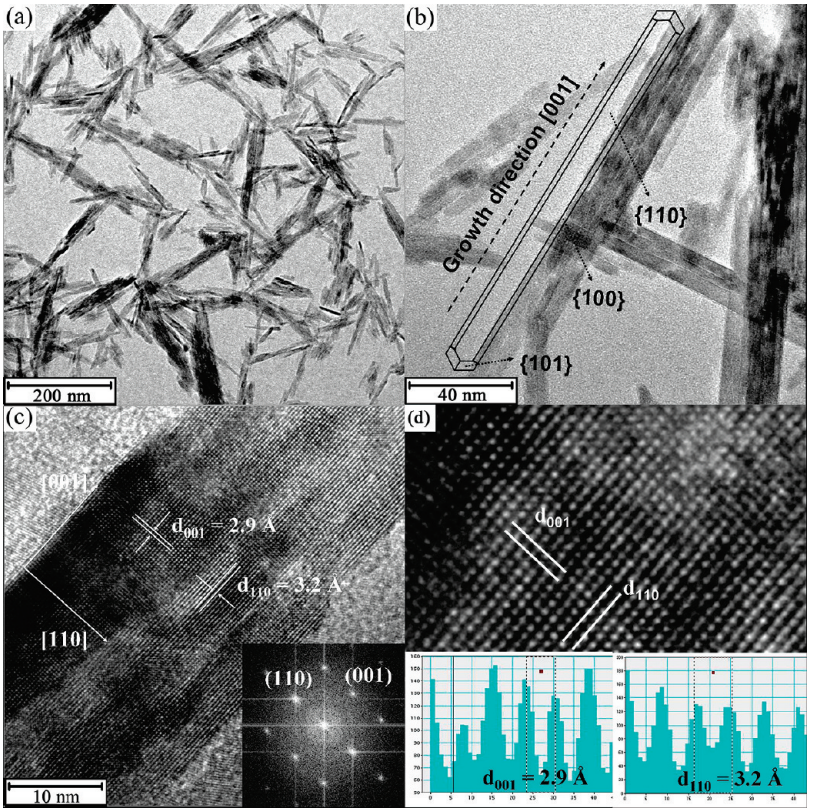

Figure 1. (a and b) Typical field-emission transmission electron microscopy (FE-TEM) images of TiO_2-NW prepared by a hydrothermal method. (c) High-resolution TEM image of the TiO_2-NW representing single-crystalline faces. The inset is the fast Fourier transform (FFT) pattern. (d) Schematic illustration of the rutile TiO_2-NW growth habit.

Herein, we synthesized TiO_2 nanowires via a hydrothermal method without any surfactant and template. The TiO_2 photoelectrode with branch-type nanostructure for dye-sensitized solar cells was achieved using a seeding method with TiO_2 nanowires as seeds. The structural and photoelectrochemical properties of the TiO_2 nanowire and nanobranch electrodes were characterized using high-resolution transmission electron microscopy (HR-TEM) and fast Fourier transform (FFT), X-ray diffraction (XRD) analysis, Brunauer−Emmett−Teller (BET) analysis, and photocurrent−voltage measurement.

Experimental Section

For the TiO_2 nanowire electrode (TiO_2-NW), 8 mL of titanium(IV) isopropoxide (TTIP (97%), Aldrich) was dropped (0.16 μL/s) in 40 mL of 10 M hydrochloric acid (HCl (35%), Aldrich) with constant stirring at 25 °C for 1 h and then kept at 120 °C for 24 h. [25] After the hydrothermal process, the resulting precipitates were cooled to room temperature, washed several times with ethanol and distilled water, and then precipitated using a centrifuge at 8000 rpm. The white TiO_2 powders (1.686 g) were obtained after drying in a 50 °C oven. The TiO_2 nanobranch electrode (TiO_2-NB) was synthesized by means of a seeding method with TiO_2-nanowires as seeds. The seed-solution (12 wt %) containing TiO_2 nanowires was injected in 30 mL of 0.5 M HCl with constant stirring at 25 °C and then kept constant for 15 min. After that, 2 mL of TTIP as precursor was dropped (0.16 μL/s) in mixture solution, kept constant for 1 h, and kept at 95 °C for 4 h. The resulting precipitates were cooled to 25 °C, washed several times with ethanol and distilled water, and precipitated using centrifuge at 8000 rpm. The white TiO_2 powders (0.189 g) were obtained after drying in a 50 °C oven.

The nanostructure electrodes synthesized were characterized by field-emission transmission electron microscopy (FE-TEM) using a Philips F20 system operating at 200 kV. The FE-TEM samples were prepared by placing a drop of the nanostructure suspension in ethanol on a carbon-coated copper grid. Structural analysis of the nanostructures was carried out by an X-ray diffraction (XRD) method using a Rigaku diffractometer equipped with a Cu Kα radiation source of λ = 0.15418 nm with a Ni filter. The tube current was 100 mA with a tube voltage of 40 kV. The 2θ between 20° and 60° was explored at a scan rate of 4°/min. The surface area and porosity of the TiO_2-NW and TiO_2-NB electrodes were analyzed by a nitrogen adsorption measurement (Micromeritics ASAP 2020 adsorption analyzer).

To characterize photoelectrochemical properties of the TiO_2-NW and the TiO_2-NB, dye-sensitized solar cells were fabricated by a conventional method. The TiO_2 powders were pasted on F-doped SnO_2 (FTO) coated glass using doctor-blade method, followed by sintering at 450 °C for 30 min in air, resulting in ~7 μm thick film. The TiO_2 coated films were immersed in a solution of Ru 535 dye (N3, Solaronix Co. Ltd.) above 12 h. The dye-adsorbed TiO_2 electrodes with an active area of 0.16 cm^2 were fabricated into the sandwich-type cell using thermal adhesive films (Serlyn, 60 μm) with Pt deposited by a sputtering method as a counter electrode. The inner space was filled up with a liquid electrolyte involving 0.5 M LiI, 0.05 M I_2, and 0.5 M *tert*-butyl pyridine in methoxypropionitrile (MPN) as a redox arbiter. Photocurrent−voltage curves were obtained

(25) Oh, J.-K.; Lee, J.-K; Kim, S. J.; Park, K.-W. *J. Ind. Eng. Chem.* **2009**, *15*(2), 270–274.

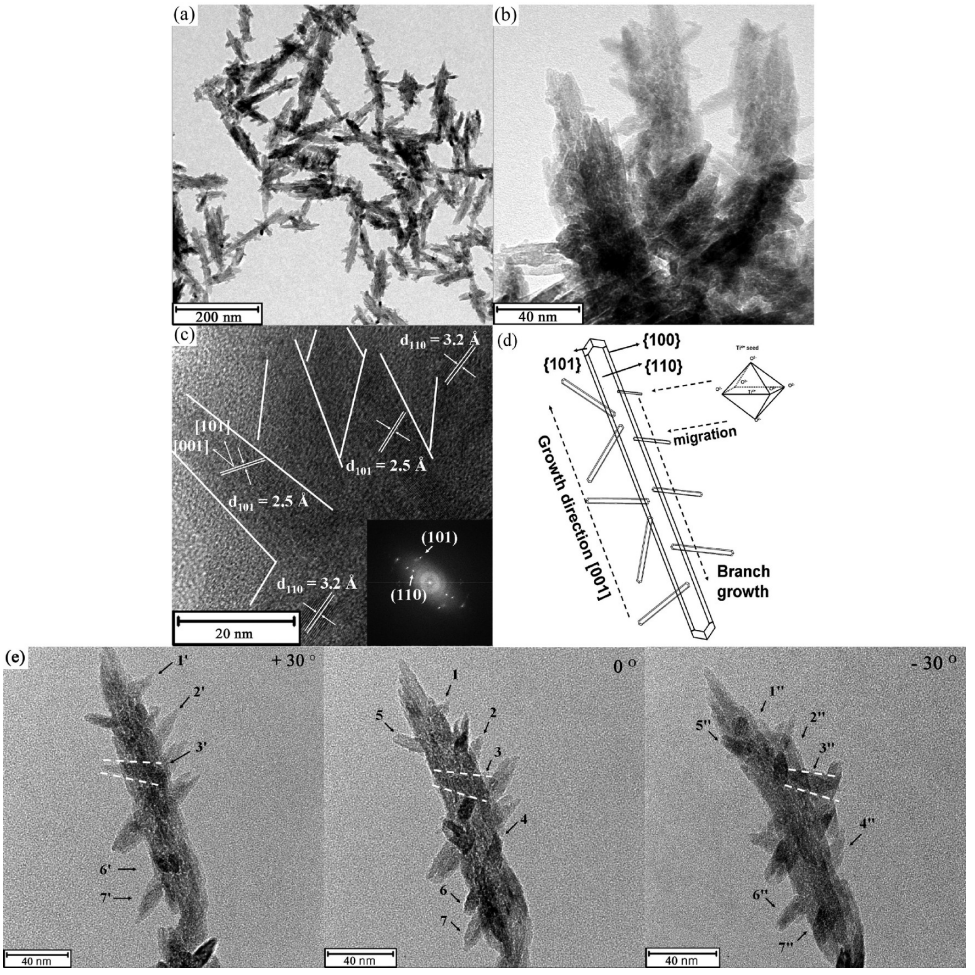

Figure 2. (a and b) FE-TEM images of TiO_2-NB synthesized by a seeding method. (c) HR-TEM image of the TiO_2-NB. The inset is the FFT pattern. (d) Schematic illustration of the formation of the rutile TiO_2-NB. (e) FE-TEM images of the TiO_2-NB tilted by ±30°.

using a 150 W xenon lamp (Sun 2000 Series Solar Simulators model 11000 source units) that was simulated AM 1.5 G solar (1 Sun condition) irradiance with an intensity of 100 mW/cm^2.

Results and Discussion

Figure 1 shows typical TEM images of TiO_2 nanoparticles obtained by means of a hydrothermal method. The as-synthesized TiO_2 nanoparticles exhibit one-dimensional nanowire structures (TiO_2-NW). The diameter and length of the TiO_2-NWs are ~8.6 and ~127.6 nm (Figure 1a and b), respectively. The phase and crystal structure of the TiO_2-NWs are confirmed by the lattice image of Figure 1c. The distance between lattice fringes is assigned to (110) and (001) of the rutile TiO_2 phase. The crystalline distances are exactly consistent with d_{110} = 3.2 Å and d_{001} = 2.9 Å of the tetragonal rutile TiO_2 phase,[10,15,26] suggesting that the TiO_2-NWs are grown along [001] axis. The inset of the Figure 1c shows fast the Fourier transform (FFT) pattern of the TiO_2-NW, which represents a single crystal of the rutile TiO_2-NW. As shown in Figure 1d, it is also confirmed that the

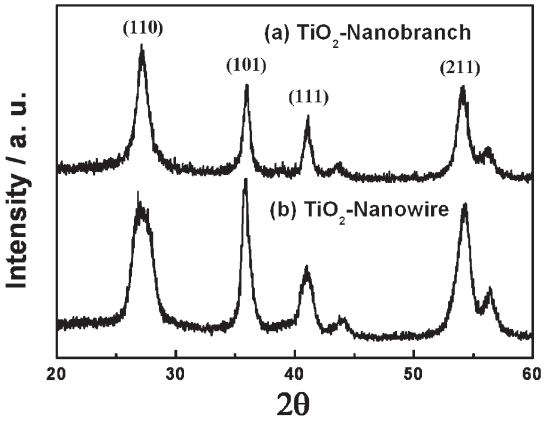

Figure 3. X-ray diffraction (XRD) patterns of TiO_2-NW and TiO_2-NB.

d-spacings of the (110) and (001) planes in the rutile TiO_2-NWs are 3.2 and 2.9 Å, respectively.

The direction of the crystal face with the corner of the coordination polyhedron occurring at the interface is favorable for a fast growth rate. Furthermore, the direction of the crystal face with the edge of the coordination polyhedron occurs at the interface the second fastest, and the direction of the crystal face with the face of the coordination polyhedron occurs at the interface, the

(26) Wang, D.; Choi, D.; Yang, Z.; Viswanathan, V. V.; Nie, Z.; Wang, C.; Song, Y.; Zhang, J.-G.; Liu, J. *Chem. Mater.* **2008**, *20*(10), 3435–3442.

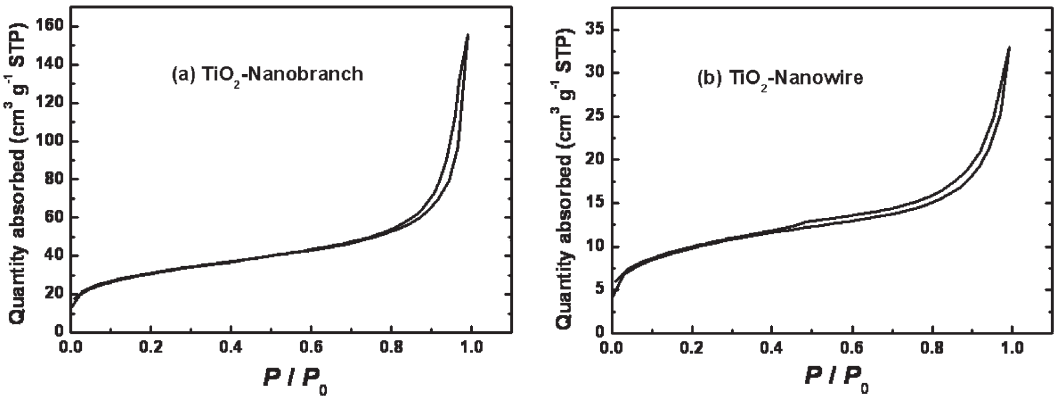

Figure 4. Nitrogen adsorption−desorption isotherm curves of (a) TiO_2-NB and (b) TiO_2-NW, respectively.

Table 1. Characteristics of as-Synthesized TiO_2-NB and TiO_2-NW Powders

samples	porosity (%)[a]	BET (m^2/g)	pore size (nm)	dye uptake (cm^{-2})[b]	roughness factor (μm^{-1})[c]
TiO_2-NB	47.2	108.5	8.9	2.9×10^9	240.6
TiO_2-NW	15	33.6	6.1	4.5×10^8	120

[a] The porosity of these samples was calculated by the following equation:[27] porosity (P) = $V_p/(\rho^{-1} + V_p)$ where V_p = the specific cumulative pore volume (cm^3/g) and ρ^{-1} = the inverse of the density of rutile TiO_2 ($\rho^{-1} = 0.238$ cm^3/g). [b] Dye uptake per unit geometric area (0.2 cm^2) is calculated by the dissolution of dye adsorbed TiO_2 film in the 1 M NaOH solution with an extinction coefficient of $\varepsilon = 14\,800$ M^{-1} cm^{-1} at 534 nm (N3 dye) using UV−vis spectroscopy. [c] The roughness factor per unit film thickness is calculated using the following equation:[27,28] roughness factor (R) = $\rho(1 - P)S$ where ρ = the density of rutile TiO_2 (ρ = 4.2 g/cm^3), P = the porosity of the sample, and S = the specific surface area (m^2/g).

slowest. The order of growth rate of rutile TiO_2 structure is $V_{\langle 110\rangle} < V_{\langle 100\rangle} < V_{\langle 101\rangle} < V_{\langle 001\rangle} < V_{\langle 111\rangle}$. Accordingly, the {001} and {111} faces disappear while {110}, {100}, and {101} faces are easily exposed during the growth process,[18] which are consistent with the TEM image and FFT pattern in Figure 1c.

Figure 2a and b show the TEM images of TiO_2 nanoparticles obtained by a seeding method using TiO_2-NWs as seeds (Figure 1). The TiO_2 nanoparticles seem to be a three-dimensional structure with branches (TiO_2-NB) grown along backbones of the TiO_2-NWs. The diameter and length of the TiO_2-NBs are ∼20 and ∼150 nm, respectively. As shown in Figure 2c of the high-resolution TEM image of the TiO_2-NB, the branches are exposed to the (101) plane of d = 2.5 Å. The branches were grown to the one-dimensional structure along [001] axis. The backbone of the TiO_2-NWs was exposed to (110) plane corresponding to d-spacing of 3.2 Å. The FFT pattern of the inset in the Figure 2c indicates the (101) and (110) plane of rutile phases, which the (001) is tilted 33° with the (101) and perpendicular to the (110). The schematic illustration of the formation of TiO_2-NB structures, based on the FE-TEM results, is presented in Figure 2d. The nucleation precursors in hydrochloric acid solution migrate into the TiO_2-NWs as seeds, where nucleation occurs at energetically favorable sites. It is likely that, as observed in the Figure 2c, the nucleus is grown in the branch shape with rutile phase and is not more favorable for the backbone growth of the TiO_2-NW. To characterize and confirm three-dimensional nanostructure of the TiO_2-NB, as shown in Figure 2e of FE-TEM images, the TiO_2-NB was rotated with the angle of ±30°. The terms +30° (TiO_2-NB(+30°)) and −30° (TiO_2-NB(−30°)) indicate right and left rotation of the centered image (TiO_2-NB(0°)) of the TiO_2-NB, respectively. In the case of the tilt from 0° to +30°, the branches marked as 1, 2, and 7 of the TiO_2-NB(0°) clearly appear as shown in 1′, 2′, and 7′ of the TiO_2-NB(+30°). The branch marked as 3 moves at the left as shown in 3′ of the TiO_2-NB(+30°) whereas the branch marked as 6 disappears. In the case of the tilt from 0° to −30°, the branches marked as 1 and 2 of the TiO_2-NB(0°) disappear as shown in 1″ and 2″ of the TiO_2-NB(−30°) whereas the branches marked as 4 and 6 of the TiO_2-NB(0°) remarkably appear as shown in 4″ and 6″ of the TiO_2-NB(−30°). As a result, from the TEM analysis, it is evident that the branches of the TiO_2-NB are three-dimensionally grown along the backbone of the TiO_2-NW.

Figure 3 shows XRD patterns of the TiO_2-NW and TiO_2-NB representing the rutile phase with tetragonal crystal structure ($a = b$ = 0.452 nm, c = 0.294 nm, space group $P4_2/mnm$). For the TiO_2-NW, since the growth rate on the (101) is faster than that on the (110), as already observed in Figure 1, the peak intensity of the (101) is even higher than the (110). However, according to the reference (JCPDS No. 88-1175) of the TiO_2 rutile phase, the intensity ratio of principal planes such as (110), (101), and (100) is 100, 50, and 60, respectively. On the other hand, the TiO_2-NB shows the similar intensity ratio of the principal XRD peaks to that of the reference in comparison with the TiO_2-NW. This also represents that the branches with rutile phase in the TiO_2-NB are formed along the (110) rather than the (101) in agreement with the TEM data of Figure 2.

Typically, a one-dimensional structure such as the TiO_2-NW is favorable for an electronic conduction and unfavorable for photonic penetration due to the difficulty of vertical arrangement of the NW. In addition,

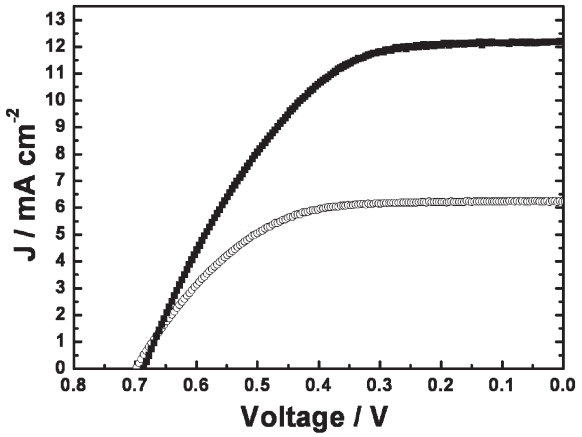

Figure 5. Photocurrent−voltage curves measured using TiO_2-NB (■) and TiO_2-NW (○) as photoelectrodes.

compared to typical spherical nanoparticles, the dye adsorption site in the TiO_2-NW is reduced resulting in a decreased photocurrent density.[19−21] Thus, it is expected that the TiO_2-NB with branched nanostructures could exhibit such an increased specific surface area for an improved photocurrent harvest efficiency. To characterize surface area, porosity, and roughness factor of the nanostructured TiO_2, the Brunauer−Emmett−Teller (BET) curves were obtained using the TiO_2-NW and TiO_2-NB as shown in Figure 4. As summarized in Table 1, the BET specific surface area of the TiO_2-NB is 108.5 m^2/g and is much larger than that of the TiO_2-NW (33.6 m^2/g). The roughness factor, defined as units of surface area per micrometer of the film thickness, of the TiO_2-NB is 240.6 and larger than 120 μm^{-1} of the TiO_2-NW. It is likely that the increased surface area and roughness factor of the TiO_2-NB could result in the high dye uptake of the TiO_2 photoanode layer improving a charge harvesting efficiency. Also, as shown in Figure 4, the initial rise in the curve is due to adsorbing molecules interacting with the most energetic regions of the solid surface and then with the less energetic regions.[27−31] Thus, it is expected that the amount of chemisorptions

(27) Nakade, S.; Kanzaki, T.; Wada, Y.; Yanagida, S. *Langmuir* **2005**, *21*(23), 10803–10807.
(28) Benkstein, K. D.; Kopidakis, N.; van de Lagemaat, J.; Frank, A. J. *J. Phys. Chem. B* **2003**, *107*(31), 7759–7767.
(29) Kang, S. H.; Kang, M.-S.; Choi, S.-H.; Kim, J.-Y.; Kim, H.-S.; Hyeon, T.; Sung, Y.-E. *Electrochem. Commun.* **2008**, *10*(9), 1326–1329.
(30) Park, N.-G.; van de Lagemaat, J.; Frank, A. J. *J. Phys. Chem. B* **2000**, *104*(38), 8989–8994.
(31) Webb, P. A.; Orr, C. *Analytical Methods in Fine Particle Technology*; Micromeritics Instrument Corp.: Norcross, GA, 1997.

Table 2. Comparison of Parameters of the Dye-Sensitized Solar Cell (DSSC) Based on TiO_2-NB and TiO_2-NW[a]

samples	V_{oc} (V)	J_{sc} (mA/cm^2)	FF	η (%)
TiO_2-NB	0.69	12.18	0.51	4.3
TiO_2-NW	0.70	6.25	0.58	2.6

[a] The J_{sc}, V_{oc}, FF, and η are short circuit current density, open circuit voltage, fill factor, and efficiency in the DSSC, respectively.

of dye molecules on the TiO_2-NB could be higher than that of the TiO_2-NW. As presented in the Table 1, the dye uptake of the TiO_2-NB is 2.9×10^9 cm^{-2} and much larger than 4.5×10^8 cm^{-2} of the TiO_2-NW.

To analyze and compare photoelectrochemical properties of the TiO_2 nanostructures in dye-sensitized solar cells, as shown in Figure 5, photocurrent−voltage curves were obtained using the TiO_2-NW and TiO_2-NB as photoelectrodes. The open-circuit voltage (V_{oc}) of the TiO_2 electrodes is almost similar due to the rutile phase of both the nanostructures. As indicated in Table 2, short-circuit current density (J_{sc}) and cell efficiency (η) of TiO_2-NW and TiO_2-NB increase from 6.25 to 12.18 mA/cm^2 and from 2.6 to 4.3%, respectively. The improved J_{sc} and η of the TiO_2-NB might be due to both increased specific surface area and roughness factor as already indicated in the BET analysis of the Figure 4 and Table 1. However, in contrast, it is likely that the fill-factor of the TiO_2-NB with grain boundaries caused by branches is lower than that of the TiO_2-NW with single crystalline structure.

Conclusions

In summary, the TiO_2 branched nanoparticle (TiO_2-NB) is synthesized by means of a seeding method with a TiO_2 nanowire (TiO_2-NW) as a seed. The as-synthesized TiO_2-NB shows a three-dimensional branched structure grown along the backbones of the TiO_2 nanowire resulting in both high specific surface area and thus improved charge harvesting efficiency. In terms of the photoelectrochemical properties of TiO_2-NB with such a three-dimensional nanostructure, both improved short-circuit current density and cell efficiency would be due to increased specific surface area and roughness factor in comparison with the TiO_2-NW.

Acknowledgment. This work was supported by the Korea Research Foundation Grant funded by the Korean Government (KRF-2008-331-D00124), Human Resource Training Project for Strategic Technology, and Manpower Development Program for Energy & Resources supported by the Ministry of Knowledge and Economy.